Research Square

Preprints are preliminary reports that have not undergone peer review.
They should not be considered conclusive, used to inform clinical practice,
or referenced by the media as validated information.

Phosphatidylinositol 3-phosphate binding to the FYVE domain of Phafin2 relieves PH domain autoinhibition mediated by the polyD motif

Marija Corluka
Fralin Life Sciences Institute, Virginia Tech
Wenhan Guo
University of Texas at El Paso
Emery Ng
Fralin Life Sciences Institute, Virginia Tech
Tuoxian Tang
Fralin Life Sciences Institute, Virginia Tech
Mahmudul Hasan
Fralin Life Sciences Institute, Virginia Tech
Lin Li
University of Texas at El Paso
Daniel G. S. Capelluto
capellut@vt.edu

Fralin Life Sciences Institute, Virginia Tech

Article

Keywords: Phafin2, PH domain, FYVE domain, autoinhibition, phosphatidylinositol 3-phosphate, phosphatidylinositol 4-phosphate, oligomerization, membrane tethering

Posted Date: November 23rd, 2026

DOI: https://doi.org/10.21203/rs.3.rs-11706191/v1

License: This work is licensed under a Creative Commons Attribution 4.0 International License.
Read Full License

Additional Declarations: No competing interests reported.

Abstract

Macropinocytosis enables nonselective uptake of extracellular fluid and macromolecules and contributes to immune surveillance, nutrient acquisition, pathogen entry, and disease progression. Phosphoinositides recruit adaptor proteins required for macropinosome formation and maturation. One such adaptor, Phafin2, associates with macropinosomes in two sequential phases, but its membrane-binding mechanism remains unclear. Phafin2 contains a PH domain that binds phosphatidylinositol 4-phosphate (PtdIns4P) and a FYVE domain that specifically recognizes phosphatidylinositol 3-phosphate (PtdIns3P). Here, we show that a C-terminal polyaspartic (polyD) motif autoinhibits the PH domain by binding it directly (K_D ≈ 4 μM) at a positively charged surface that includes K51 and R53, residues also required for PtdIns4P binding. HDX-MS and normal mode analysis indicate that the tail occludes this site and restrains PH-FYVE interdomain motion, stabilizing a closed conformation. FYVE binding to PtdIns3P allosterically enables PH domain binding to PtdIns4P, producing cooperative lipid recognition on macropinosome-sized liposomes. Phafin2 oligomerized on PtdIns3P, did not oligomerize on PtdIns4P alone, and oligomerized more strongly when both lipids were present. Phosphomimetic substitution of S239, S247, and S248 reduced PtdIns3P binding, cooperativity, and oligomerization, and MD simulations suggest that phosphorylation compacts the tail against the PH-FYVE interface, reinforcing autoinhibition. Liposome clustering paralleled oligomerization, with fewer liposomes tethered by PtdIns3P alone than by PtdIns3P and PtdIns4P together. In cells, Phafin2 is known to associate with macropinosomes that accumulate but do not fuse during the first phase, when both lipids are present. Dual-lipid engagement may therefore hold first-phase macropinosomes in a tethered, fusion-restricted state, whereas loss of PtdIns4P would weaken tethering and permit fusion. Together, these data support a sequential dual-domain mechanism in which FYVE-PtdIns3P binding relieves PH domain autoinhibition, coupling lipid coincidence detection to membrane tethering.

Introduction

Macropinocytosis is an actin-driven endocytic process in eukaryotic cells that facilitates the nonselective uptake of fluids and macromolecules [1]. It begins at the cell surface with the formation of actin-dependent membrane ruffles, followed by their closure into a macropinocytic cup. This cup subsequently closes and detaches from the plasma membrane, forming a nascent macropinosome, a large vesicle of 0.2-5 μm [1]. As the macropinosome matures, it undergoes changes in both shape, size, and molecular composition. During these transitions, macropinosomes generate recycling tubules that return non-degradable material to the plasma membrane by exocytosis. Macropinosomes first acquire early endosomal identity and then transition to late endosomal identity, ultimately fusing with endolysosomes or lysosomes for cargo degradation. The resulting breakdown products are released into the cytoplasm, where they support cell growth and survival.

Macropinosome formation and maturation are regulated by stage-specific phosphoinositide remodeling that recruits effector proteins to coordinate membrane dynamics [2]. Phafin2 is required for this process;

its depletion impairs macropinosome internalization and maturation [1,2]. Phafin2 contains an N-terminal PH domain that preferentially binds phosphatidylinositol 4-phosphate (PtdIns4P) and a central FYVE domain that binds phosphatidylinositol 3-phosphate (PtdIns3P) [reviewed in [3]]. Unlike many dual-domain phosphoinositide effectors, Phafin2 harbors a C-terminal polyD motif that autoinhibits PH-domain lipid engagement while preserving FYVE-mediated PtdIns3P binding [4]. This architecture suggests a conformationally gated mechanism in which FYVE-dependent membrane engagement relieves this inhibition and activates the PH domain, enabling coordinated dual-lipid sensing. However, the structural basis for this allosteric regulation remains unknown.

Phafin2 exhibits two distinct waves of membrane association during macropinocytosis [5]. In the first phase, it associates with irregularly shaped, nascent macropinosomes coated with an actin-dense network. This association requires coincidence detection of PtdIns4P by the PH domain and PtdIns3P by the FYVE domain. During this phase, the proposed primary role of Phafin2 is to destabilize the actin-dense network, a process facilitated by its binding to actin and the actin accessory protein Filamin A (Fil A) *via* its PH domain. During the second phase, Phafin2 binds to the rounded early macropinosomes. In this phase, the protein's membrane association depends solely on the FYVE domain, as these organelles are enriched exclusively in PtdIns3P, facilitating recycling by the formation of tubular structures, in coordination with the microtubule-associated protein JIP4 [6], upon macropinosome shrinking and changes in shape [7].

The AlphaFold-predicted structure of Phafin2 suggests that the polyD motif is positioned between the PH and FYVE domains and stabilized by electrostatic interactions. Here, we show that the polyD motif directly interacts with the PH domain with moderate affinity at a site that overlaps with its phosphoinositide-binding interface, and weakly with the FYVE domain, supporting a modulatory role for membrane binding. Hydrogen-deuterium exchange mass spectrometry (HDX-MS) further reveals that both the putative phosphoinositide-binding site within the PH domain and a nonconserved electrostatic region within the FYVE domain are buried in Phafin2, consistent with an autoinhibited conformation. Molecular dynamics (MD) simulations further indicate that the PH and FYVE domains undergo open-closed conformational motions. We further show that Phafin2 is unable to associate with PtdIns4P in the absence of PtdIns3P, identifying the FYVE domain as a previously unrecognized allosteric regulator of Phafin2 binding to PtdIns4P. Binding of the FYVE domain to PtdIns3P releases the autoinhibitory polyD-PH interaction, thereby enabling curvature-dependent membrane engagement. PtdIns3P binding triggers the assembly of Phafin2 into large oligomeric complexes, a process that is strongly enhanced when both PtdIns3P and PtdIns4P are present. Consistent with this molecular rearrangement, Phafin2 markedly clusters liposomes enriched with both PtdIns3P and PtdIns4P, indicating that it can tether membranes *in vitro*. Phafin2 is phosphorylated at residues S239, S247, and S248 [8], which are located in and around the polyD motif. In the presence of PtdIns3P, a phosphomimetic Phafin2 mutant displays reduced PtdIns4P binding, decreased oligomerization, and reduced liposome tethering, consistent with increased electronegativity of the polyD motif shifting the conformational equilibrium toward the closed state. Collectively, these findings support a model in which Phafin2 exists in a dynamic equilibrium

between closed (autoinhibited) and open (membrane-bound) conformations. In this model, the FYVE domain functions as an allosteric regulator that senses PtdIns3P and releases polyD-mediated inhibition of the PH domain, enabling membrane engagement. This mechanism provides a framework for the dual PtdIns3P and PtdIns4P dependence of Phafin2 on nascent macropinosomes, where PtdIns4P is enriched at the plasma membrane whereas PtdIns3P is generated locally during macropinosome formation. We propose that the PtdIns3P present together with PtdIns4P on nascent macropinosomes allosterically activates Phafin2, enabling dual phosphoinositide engagement and membrane tethering that may contribute to the lack of homotypic fusion at this phase.

Results

The polyD motif directly and preferentially interacts with the PH domain over the FYVE domain. Removal of the C-terminal polyD region of Phafin2 (Fig. 1a) increased PH-domain binding to membrane phosphoinositides [4]. To test whether this reflects a direct intramolecular interaction, we measured binding of a synthetic polyD peptide to the isolated PH and FYVE domains by isothermal titration calorimetry (ITC). The peptide bound the PH domain with moderate affinity (K_D of 4.1 μM) but the FYVE domain only weakly (K_D ≈ 350 μM) (Fig. 1b-c, f; **Suppl. Table 1**). Saturable quenching of PH-domain tryptophan fluorescence (W100 and W122) upon peptide titration yielded a consistent K_D of 4.2 μM (**Suppl. Figure 1a**)., in agreement with the affinity measured by ITC. The polyD motif did not bind the PH domain of AKT1, a known Phafin2 interactor [9] (**Suppl. Figure 1b**), indicating specific autoinhibition of Phafin2.

To further investigate intramolecular regulation of Phafin2 by the polyD motif, we performed ^{1}H-^{15}N heteronuclear single quantum coherence (HSQC) NMR experiments to map chemical shift perturbations in the PH domain upon addition of the polyD peptide, using the published backbone resonance assignments of the domain [10]. Several residues exhibited significant perturbations, including the conserved residues G38, K44, L45, K51, A52, R53, I67, I90, K91, T104, F109, and A110 (Fig. 1g and **Suppl. Figure 1c**). These residues cluster mainly within the β-sheet core of the PH domain (Fig. 1h), including R53, which has previously been shown to be critical for PtdIns3P binding by the Phafin2 PH domain [4,5]. To test whether these polyD-contacting residues also contribute to PtdIns4P-dependent membrane binding, we performed liposome co-sedimentation assays using the isolated PH domain. The wild-type PH domain bound efficiently to PtdIns4P-containing liposomes, whereas the K51A/R53C mutant showed significantly reduced binding (Fig. 1i). These results indicate that K51 and R53, in addition to mediating polyD engagement, are also important for PH domain association with PtdIns4P-containing membranes.

Consistent with the NMR mapping, the PH domain mutant K51A/R53C failed to interact with the polyD peptide (Fig. 1d), supporting a shared interaction surface for polyD and phosphoinositide binding. The polyD peptide bound Phafin2 ΔpolyD with a K_D of ≈ 12 μM (Fig. 1e), ~ 3-fold weaker than the isolated PH domain (Fig. 1f and **Suppl. Table 1**). This reduction might reflect the FYVE domain partially limiting access to the PH domain.

The phosphoinositide-binding site in the PH domain is occluded by the polyD motif. Because no experimentally determined structure of Phafin2 exists, HDX-MS was carried out to probe local backbone dynamics across its domains and motifs. Peptic digestion yielded 106 peptides with a sequence coverage of 100% and an average redundancy of 7.56, providing sub-peptide spatial resolution across the majority of the Phafin2 sequence (**Suppl**. **Data 1**). The observed exchange pattern was broadly consistent with the AlphaFold-predicted structural model. The PH and FYVE domains each contained regions of slow, intermediate, and rapid deuterium uptake, whereas the C-terminal tail, including the polyD motif, displayed intermediate HDX kinetics (Fig. 2a, **top heatmap**). Within the PH domain, regions encompassing residues 46–66 and 119–129 exhibited low levels of deuterium incorporation (Fig. 2a, **top heatmap**), indicating limited solvent accessibility and suggesting a structurally stable core. Consistent with NMR chemical shift perturbation data (Fig. 1g-h), which indicate that the polyD motif interacts with a positively charged surface of the PH domain (residues K44, L45, K51, A52, and R53), these findings support a model in which intramolecular contacts restrict solvent exposure and potentially mediate an autoinhibitory conformation that limits phosphoinositide binding. In contrast, the majority of the FYVE domain displayed high deuterium incorporation (Fig. 2a, **top heatmap**, and **2b**), consistent with increased solvent exposure and/or conformational flexibility. The primary protected region within this domain spanned residues 168–180, encompassing the conserved RRHHCR motif, which is known to mediate recognition of the 3-phosphate and hydroxyl groups at the 4- and 5-positions of PtdIns3P [11]. Conversely, two additional regions implicated in PtdIns3P binding, 149-WVPD-152 and 201-RIC-203, exhibited high exchange rates (Fig. 2a, **top heatmap**), suggesting that these segments remain solvent-accessible and potentially dynamic under the conditions tested.

To evaluate the contribution of the polyD motif to the conformational state of Phafin2, HDX-MS analysis was performed on a deletion mutant lacking this motif (Phafin2 ΔpolyD). Peptic digestion of Phafin2 ΔpolyD yielded 97 peptides with a sequence coverage of 100% and an average redundancy of 6.46 (**Suppl**. **Data 2**), permitting direct comparison with the wild-type dataset across the shared sequence. Removal of the polyD motif resulted in markedly increased deuterium incorporation across the protein (**Suppl. Figure 2a**), consistent with a global conformational change, and in agreement with near-UV circular dichroism data indicating altered tertiary structure upon polyD deletion (**Suppl. Figure 2b**). Strikingly, and in contrast to wild-type Phafin2, the phosphoinositide-binding site of the PH domain, as well as its C-terminal flanking region, became less buried in the deletion mutant (Fig. 2a, **bottom heatmap**). The linker region and the N-terminal portion of the FYVE domain, which harbors the WVPD motif, were less solvent-exposed in Phafin2 ΔpolyD, whereas the remaining two PtdIns3P-contacting regions, the RRHHCR motif and the 201-RIC-203 segment, retained exchange profiles comparable to those observed in wild-type Phafin2 (Fig. 2a). HDX-MS analysis of the difference in deuterium incorporation (Phafin2 ΔpolyD minus Phafin2) revealed predominantly increased exchange in the ΔpolyD protein, with the exception of the linker between the PH and FYVE domains and the WVPD and RRHHCR motifs, which showed decreased deuterium incorporation, indicating increased protection in these regions upon polyD deletion (**Suppl. Figure 2a** and **c**). Collectively, these findings demonstrate that the polyD motif is a critical determinant of Phafin2 conformational architecture, enforcing an autoinhibited

state in which the PH domain lipid-binding interface is occluded. Its removal redistributes solvent accessibility across both domains in a manner consistent with relief of intramolecular restraint, further supporting the model in which polyD-mediated contacts with the PH domain gate phosphoinositide engagement.

The C-terminal tail, including the polyD motif, restricts the PH-FYVE domain opening and closing conformations in Phafin2. To examine the structural basis of the conformational restraint revealed by HDX-MS, we performed normal mode analysis (NMA) [12] on tail-containing and tail-free Phafin2 (residues 1-212) models to evaluate how the C-terminal polyD tail influences large-scale PH-FYVE interdomain dynamics. In the tail-containing model, the polyD motif lay along the PH-FYVE interface, with smaller, more uniformly oriented vectors in both domains and the largest displacements confined to the distal end of the tail (Fig. 2d, left). In the tail-free model, the PH and FYVE domains showed prominent, divergently oriented vectors, indicating coupled interdomain motion (Fig. 2d, right). Quantitatively, the tail-free model showed a PH-FYVE center-of-mass distance range of 3.52 Å and an interdomain axis angle range of 58.77°, which the tail reduced to 0.80 Å and 42.67° (**Suppl. Figure 3**). Thus, the C-terminal tail acts as a conformational restraint, limiting interdomain opening and closing. In agreement with the HDX-MS data demonstrating occlusion of the PH domain lipid-binding interface in full-length Phafin2, the NMA results suggest that this dynamic restriction is mechanistically coupled to autoinhibition with tail-mediated dampening of interdomain reorientation limiting the conformational states required for productive PtdIns4P engagement at the macropinosomal membrane.

The FYVE domain allosterically regulates Phafin2 binding to PtdIns4P. Because membrane curvature can influence recruitment of peripheral membrane proteins [13–15], we next tested whether Phafin2 binding depended on vesicle size. Liposomes containing both PtdIns3P and PtdIns4P, or PtdIns3P alone, were prepared by extrusion through polycarbonate membranes (50–400 nm pore sizes). Phafin2 preferentially bound dual-lipid low-curvature membranes extruded through 200–400 nm pores (**Fig. 3a**), consistent with the estimated diameter range of macropinosomes, which are ≥ 200 nm [16], whereas its binding to PtdIns3P-only liposomes did not depend on vesicle size (**Suppl. Figure 4**). This preference for low-curvature membranes in the presence of both lipids suggests that membrane geometry, together with phosphoinositide composition, helps restrict Phafin2 recruitment to macropinosomes.

Because Phafin2 bound significantly over 200 nm vesicles, we used 400-nm liposomes, which fall within the macropinosome size range, for all subsequent binding assays. Under these conditions, liposome co-sedimentation assays showed that Phafin2 bound selectively to phosphoinositide-enriched membranes (**Fig. 3b**). Phafin2 associated with liposomes containing PtdIns3P, consistent with engagement of the FYVE domain (**Suppl. Figure 5a**), whereas PtdIns4P alone showed negligible association. Strikingly, liposomes containing both PtdIns3P and PtdIns4P produced significantly enhanced binding, indicating cooperative recognition of the two phosphoinositides, in agreement with previous observations [5].

Mutation of the PtdIns3P-binding site within the FYVE domain (R171A/R172A) disrupted PtdIns3P association and also reduced PtdIns4P binding by the PH domain (**Fig. 3c**), consistent with an allosteric

mechanism in which FYVE domain engagement promotes PH domain lipid recognition. Removal of the polyD region resulted in measurable PtdIns4P binding, with an additive effect when liposomes contained both PtdIns3P and PtdIns4P (**Fig. 3d**). This PtdIns4P binding persisted even when the same construct carried an inactivating mutation in the FYVE domain (**Suppl. Figure 5b**), indicating that, in the absence of the polyD region, PH domain binding to PtdIns4P no longer requires FYVE-mediated PtdIns3P engagement. The binding was similar in magnitude to that observed for the isolated PH domain (**Suppl. Figure 5c**) and was nearly abolished in the K51A/R53C mutant (**Suppl. Figure 5d**), confirming that it depends on the same lipid-binding surface used for PtdIns4P-dependent recognition. Together, these results indicate that the polyD region restrains PH domain interaction with PtdIns4P, whereas FYVE domain binding to PtdIns3P promotes it, thus, establishing opposing regulatory inputs that jointly control PH domain lipid binding.

Figure 3. Intramolecular allosteric regulation and PtdIns3P-dependent oligomerization of Phafin2 mediated by the FYVE domain. (**a)** Left, binding of Phafin2 to the indicated liposome sizes containing both PtdIns3P and PtdIns4P. Right, densitometric quantification of the bound fraction. S, supernatant; P, pellet. *, $p < 0.1$; ***, $p < 0.001$. **(b-d**) Left, binding of Phafin2 (**b**), Phafin2 R171A/R172A (**c**) and Phafin2 ΔpolyD (**d)** to 400-nm liposomes containing the indicated phosphoinositides. Right, densitometric quantification of the bound fraction. In all panels, S, supernatant; P, pellet. **, $p < 0.01$. (**e-h**) Crosslinking assays of Phafin2 (**e**), Phafin2 ΔpolyD (**f**), Phafin2 R171A/R172A ΔpolyD (**g**), and Phafin2 S239D/S247D/S248D (**h**). Constructs were incubated with the indicated liposomes in the absence or presence of BS^3, and the samples were then run on SDS-PAGE

Phafin2 oligomerizes in a PtdIns3P-dependent manner. Beyond its role in phosphoinositide recognition, the Phafin2 PH domain has also been reported to interact with F-actin and Filamin A, an interaction network required for the release of nascent macropinosomes from the underlying cortical actin cytoskeleton [5,6]. However, given the size and complexity of these ligands, that is actin filaments, Filamin A bound to actin, and PtdIns4P embedded within the plasma membrane, it seems unlikely that a single Phafin2 monomer [17] could bind all three simultaneously to drive macropinosome release. Because membrane binding may promote Phafin2 oligomerization, enabling multivalent interactions with actin and phosphoinositides that monomers cannot achieve, we tested whether Phafin2 oligomerizes in a phosphoinositide-dependent manner. To test this, Phafin2 was incubated with liposomes containing PtdIns3P, PtdIns4P, or both, and protein complexes were cross-linked using bis(sulfosuccinimidyl) suberate (BS^3). In contrast to liposomes containing PtdIns4P alone, Phafin2 formed large complexes in the presence of PtdIns3P-containing liposomes, and the abundance of these complexes increased further when both phosphoinositides were present (**Fig. 3e**). These data suggest that binding of the FYVE domain to PtdIns3P promotes Phafin2 oligomerization, which is further sequentially enhanced by PH domain interaction with PtdIns4P. A similar outcome was observed when the polyD motif was deleted from Phafin2 (**Fig. 3f**), indicating that FYVE-PtdIns3P interactions provide the primary driving force for Phafin2 oligomerization. Consistent with this interpretation, Phafin2 carrying an inactive FYVE domain (R171A/R172A) failed to oligomerize in the presence of PtdIns3P (**Suppl. Figure 6**). Strikingly,

when the R171A/R172A mutation was combined with deletion of the polyD motif, the resulting construct failed to oligomerize with either phosphoinositide (**Fig. 3g**). This indicates that relieving polyD-mediated restraint on the PH domain is not sufficient to drive oligomerization in the absence of FYVE-PtdIns3P interaction and confirms that FYVE domain binding to PtdIns3P is required to initiate the oligomerization process, independent of the regulatory role of the polyD motif.

Phosphorylation of the polyD-tail reduces FYVE domain binding to PtdIns3P. Having established that the polyD motif regulates PH domain-mediated PtdIns4P binding, we next asked whether a related electrostatic mechanism might also modulate FYVE domain association with PtdIns3P. Although Phafin2 contains several potential phosphorylation sites, two independent studies have identified S239, S247, and S248 as phosphorylated residues by an as-yet-unidentified serine/threonine kinase [8,18]; of these, S247 and S248 lie within the polyD motif itself, whereas S239 lies immediately upstream. To evaluate the functional consequences of these phosphorylations, we generated a phosphomimetic Phafin2 construct in which all three serine residues were replaced with aspartate. Liposome co-sedimentation assays revealed that the phosphomimetic protein exhibited significantly reduced PtdIns3P binding, with a concomitant loss of binding cooperativity (Fig. 4a). Consistent with this, PtdIns3P-dependent oligomerization of Phafin2 was likewise reduced in the phosphomimetic construct (**Fig. 3e** and **h**). Together, these results suggest that phosphorylation of Phafin2 attenuates the PtdIns3P-binding activity of the FYVE domain. To further validate this observation, we computed the surface electrostatic potential of nonphosphorylated and phosphorylated Phafin2, at residues S239, S247, and S248, using DelPhi. In both proteins, the negatively charged polyD motif was flanked by a region of pronounced positive surface potential; however, the phosphorylated protein displayed an extension of negative surface electrostatic potential toward the N-terminus (Fig. 4b). The S239D/S247D/S248D phosphomimic showed a more negative electrostatic potential than the unmodified protein, although less pronounced than that of Phafin2 phosphorylated at the same residues (**Suppl. Figure 7a)**. Taken together, these findings indicate that phosphorylation of Phafin2 induces local conformational changes within the PH domain that generate an electrostatically unfavorable environment for PtdIns3P interaction.

Unlike wild-type Phafin2, the phosphomimic mutant showed greater resistance to limited trypsin proteolysis (Fig. 4c), indicating a more closed conformation, in line with its reduced binding to PtdIns3P-containing liposomes (Fig. 4a). MD simulations further showed that the unphosphorylated tail is highly flexible, whereas phosphorylation at S239, S247, and S248 constrains its motion and stabilizes it at the PH-FYVE interface (**Suppl. Figure 7b, Movies S1** and **S2**). Unexpectedly, ITC revealed that the phosphomimic and wild type bind soluble PtdIns3P with indistinguishable affinity (**Suppl. Figure 7c and Suppl. Table 2**), implying that specific recognition depends on the membrane presentation of the lipid. FYVE domains engage membranes through an insertion loop [19], and in the phosphorylated state, the simulations showed that this loop is less mobile in the phosphorylated state (**Movies S1 and S2**), which may impair PtdIns3P-dependent membrane targeting.

Analysis of ion-pair contacts showed that phosphorylation strengthens specific salt bridges between the tail and the PH domain. K44, which is involved in polyD binding (Fig. 1g), formed a salt bridge with D246 at 100% occupancy in the phosphorylated state (versus 63% when unphosphorylated), and K49-D237 occupancy rose from ~ 30% to ~ 85%. In addition, K51, a conserved PH-domain residue that binds polyD in the unphosphorylated form (Fig. 1g), shifted its interaction to tail residues D242 and D243 upon phosphorylation (**Suppl. Table 3**).

In macropinocytosis, Phafin2 associates with macropinosomes in two sequential phases. Macropinosomes in the first phase did not undergo homotypic fusion even when in extensive contact with neighboring vesicles, whereas those in the second, PtdIns3P-dependent phase fused readily upon contact [5]. Although this suggested that the two phases represent distinct steps of macropinosome maturation, whether Phafin2 itself contributes to this difference in fusion competence was not addressed. To determine how Phafin2 membrane targeting affects the behavior of lipid bilayers, specifically whether coincident lipid recognition enables Phafin2 to bridge adjacent membranes, we used confocal imaging of 800 nm fluorescent liposomes and quantified clustering by counting clusters across z-stacks. Wild-type Phafin2 clustered PtdIns3P-containing liposomes, and clustering was significantly enhanced when PtdIns4P was also present (Fig. 5, **Suppl. Figure 8**, and **Suppl Movie 3**), indicating that Phafin2 can tether membranes *in vitro* in a PtdIns3P-dependent manner and that this activity is enhanced by coincident recognition of both lipids, a dependence that parallels the lipid requirements of Phafin2's first membrane-association phase on nascent macropinosomes [5]. Conversely, the polyD phosphomimic variant showed reduced liposome clustering under both lipid conditions (Fig. 5, **Suppl. Figure 8** and **Suppl Movie 4**), consistent with the reduced PtdIns3P-binding activity of the FYVE domain (Fig. 4a), which in turn limits PH domain binding to PtdIns4P. Consistent with this, the R171A/R172A mutant also showed reduced clustering even with the polyD motif removed (Fig. 5, **Suppl. Figure 8**, and **Suppl Movie 5**). Together, these results indicate that Phafin2 can tether PtdIns3P/PtdIns4P-positive membranes *in vitro* through coincidence detection, raising the possibility that, on nascent macropinosomes, this tethering contributes to the lack of homotypic fusion observed in the first phase [5].

Discussion

PH domains are often involved in autoinhibition by folding over adjacent conserved protein modules, thereby preventing access to catalytic sites or blocking interactions with other proteins [20]. This inhibitory conformation can be relieved through specific molecular events, such as phosphoinositide binding or phosphorylation, allowing precise spatial and temporal regulation of protein function. Here, we provide evidence for a novel regulatory mechanism involving the PH domain of Phafin2. In its resting state, Phafin2 adopts a closed conformation in which the PH domain interacts with a C-terminal polyD motif, effectively restricting its accessibility. This autoinhibitory interaction is disrupted upon binding of the neighboring FYVE domain to PtdIns3P, which induces a conformational change that releases the PH domain. The released PH domain then becomes competent for simultaneous interactions primarily with PtdIns4P, enhancing membrane targeting through a synergistic mechanism involving both lipid-binding

domains. Although several protein partners have been identified for PH domains, either facilitating phosphoinositide binding or modulating PH domain function [21], this intramolecular regulation by a C-terminal polyD motif, relieved by lipid binding to a neighboring domain, represents a distinct mode of control.

HDX-MS data support this closed conformation, indicating that the polyD motif shields the PH domain, keeping it away from solvent. Deletion of the polyD motif renders the region spanning residues 46–66 more solvent accessible (Fig. 2). NMA, which identifies low-frequency collective motions encoded by protein structure [22], points to the same restraint. Under identical analysis conditions, the polyD-containing tail reduced the PH-FYVE center-of-mass distance range from 3.52 to 0.80 Å and narrowed the angular range (**Suppl. Figure 3**). Because NMA amplitudes depend on mode scaling and model setup, these values are interpreted comparatively rather than as experimental amplitudes, but they indicate that the tail restricts relative motion between the two domains. The HDX-MS results also indicate that the first lipid-contacting residues within the FYVE domain are likely the WVPD and RIC motifs, as these regions are highly solvent exposed. In EEA1, the WVPD motif uses D152 to recognize the 5' and 6' hydroxyl groups of the PtdIns3P inositol ring, whereas the arginine residue of the RVC motif (corresponding to RIC in Phafin2) participates in recognition of the 3-phosphate group [11]. We propose that initial recognition of PtdIns3P by the WVPD and RIC motifs induces a conformational change in the FYVE domain that exposes the RRHHCR region for additional contacts with the 3-phosphate group. This rearrangement may weaken the polyD motif-PH interaction, enabling phosphoinositide recognition.

Phafin2 assembles on phosphoinositide-containing membranes through a mechanism consistent with lipid-dependent stabilization of pre-existing oligomeric states. Crosslinking with BS^3 revealed an identical oligomeric binding pattern in the presence of PtdIns3P alone or in combination with PtdIns3P and PtdIns4P, indicating that the fundamental oligomerization interfaces and stoichiometries are unchanged. However, the increased intensity of higher-order oligomeric species observed upon inclusion of PtdIns4P suggests a shift in the equilibrium toward more populated and/or longer-lived assemblies. Such assembly could offer several advantages. Oligomerization would increase avidity, letting multiple FYVE and PH domains engage both lipids and making recruitment sensitive to lipid density. Because PtdIns3P promotes oligomerization and this is enhanced when PtdIns4P is also present, assembly could also give a switch-like transition from a monomeric, autoinhibited pool to a membrane-engaged state. Finally, assemblies could bridge membranes or concentrate effectors such as Filamin A, although this remains untested.

Phafin2 has been reported to interact with AKT1 [9,23], and phosphate-release assays with recombinant proteins confirmed that AKT1 phosphorylates it [24]. However, the phosphorylation site(s) within the polyD region do not match the AKT consensus motif (RxRxxS/T) [25], which suggests that a different kinase modifies this region. Phosphorylation is known to alter phosphoinositide interactions in other proteins. For example, phosphorylation of TIRAP is thought to distort its polybasic motif, reducing phosphoinositide binding and membrane targeting [26]. In the Fgd family, the central FYVE domain is

flanked by two PH domains, with a DH domain upstream of the first PH domain, and its phosphoinositide-binding function appears to be modulated by phosphorylation at several sites across this architecture [27]. Fgd3 is hyperphosphorylated on a conserved serine/threonine pair within its membrane insertion loop, a modification similar to the phosphoinositide stop mechanism in PX-domain sorting nexins, where phosphorylation of a switch residue controls PtdIns3P binding and endosomal localization [28]. In several Fgd members, phosphorylation of acidic clusters upstream of the DH domain has been proposed to relieve autoinhibition and indirectly influence FYVE domain-mediated membrane engagement [27]. In Phafin2, by contrast, the phosphorylated acidic region lies C-terminal to the FYVE domain, and our simulations suggest that it may instead reinforce autoinhibition. Consistent with a regulatory role for this region, our MD simulations identify this segment as one of the most dynamic regions of Phafin2 in the non-phosphorylated state (**Movie S1**). Phosphorylation at S239, S247, and S248 substantially suppresses the mobility of this region and promotes the formation of stabilizing electrostatic and hydrogen-bond interactions between the C-terminal tail and the PH-FYVE interface. These interactions favor a more compact and ordered conformation in which the tail is more tightly associated with the protein core.

These phosphorylation-induced contacts may provide a structural explanation for reduced PtdIns3P binding. Particularly noteworthy is the formation of a persistent hydrogen bond between S153 of the FYVE domain and L235 of the C-terminal tail. S153 is positioned immediately adjacent to the conserved WVPD motif that contributes to PtdIns3P recognition, suggesting that phosphorylation-mediated stabilization of the tail may directly influence the conformational dynamics of the lipid-binding site. This interpretation is supported by studies of the homologous FYVE domain-containing protein EEA1, where N153, the residue equivalent to Phafin2 S153, was shown by nanodisc-based binding assays and solution NMR spectroscopy to play a direct role in membrane-embedded PtdIns3P recognition [29,30]. Thus, the phosphorylation-dependent S153-L235 interaction identified here may constrain the local environment surrounding the WVPD motif and reduce its ability to engage PtdIns3P. Phosphorylation also promotes the formation of new hydrogen bonds between FYVE domain residues S197 and S198 and the terminal polyD residue D249, further strengthening tail-FYVE coupling.

Electrostatics may add to these effects. In addition to a potential direct electrostatic contribution from the phosphorylated residues themselves at the FYVE PtdIns3P-binding pocket, PH domain residues E19, E39, and D60 contribute to the same continuous electronegative surface in the folded structure. This suggests that phosphorylation of the polyD tail generates a broader, more intense negative electrostatic field spanning the PH-FYVE interface than would be predicted from the phosphosites alone, which may further disfavor engagement of the anionic PtdIns3P headgroup by the FYVE domain. Together with the extensive network of phosphorylation-enhanced salt bridges and hydrogen bonds at the PH-FYVE interface, these effects support a model in which phosphorylation stabilizes a compact, autoinhibited conformation of Phafin2 that is less competent for productive PtdIns3P binding.

Our finding that Phafin2 tethers PtdIns3P-containing liposomes, with tethering enhanced when PtdIns4P is also present, parallels a striking observation in the two-phase model of Phafin2 macropinosome

localization [5]. In that study, macropinosomes in the first phase of Phafin2 recruitment, when both PtdIns3P and PtdIns4P are present, essentially never undergo homotypic fusion despite extensive vesicle-vesicle contact, whereas second-phase macropinosomes, which contain PtdIns3P but no PtdIns4P, fuse efficiently. Between the two phases, PtdIns4P is lost and PtdIns3P is also transiently depleted. PtdIns3P is then resynthesized on early macropinosomes, triggering the second phase of Phafin2 recruitment and maturation toward endosomal identity. This inverse relationship, dual-lipid engagement coinciding with non-fusogenic contact and PtdIns3P-only engagement coinciding with fusion, raises the possibility that Phafin2, rather than promoting macropinosome fusion directly, instead uses coincidence detection of PtdIns3P and PtdIns4P to hold macropinosomes in a tethered, fusion-restricted state, with fusion proceeding only after PtdIns4P is lost and tethering is weakened. Under this model, the PH-polyD-FYVE conformational switch we describe here would not only modulate nutrient scavenging but also the timing of macropinosome fusion and the transition to recycling, coupling lipid-state sensing to a discrete maturation checkpoint. We note that this model bridges our *in vitro* tethering data with cell-based fusion observations from a distinct study, and each dataset addresses only part of the proposed mechanism. Our reconstituted system lacks the fusion machinery (Rab GTPases, SNAREs) present in cells, and the published live-cell data did not test Phafin2-dependent tethering directly. Distinguishing a genuinely restrictive tethering role from a coincidental correlation will require testing whether tethering-deficient Phafin2 mutants, such as the phosphomimic and R171A/R172A variants, cause premature fusion of first-phase macropinosomes in cells.

The sequential phosphoinositide conversions that characterize macropinosome maturation provide a spatiotemporal framework for the staged recruitment described in our model (Fig. 6). PtdIns(3,4,5)P_3 accumulation at the nascent macropinocytic cup is a well-established driver of actin remodeling and membrane ruffling [1], yet Phafin2 is not recruited at this phase [5]. The autoinhibited, closed conformation enforced by the polyD motif may effectively raises the nonspecific membrane-binding threshold of Phafin2 such that PtdIns(3,4,5)P_3 alone is insufficient for recruitment. This selectivity could temporally gate Phafin2 activity to post-closure stages, decoupling it from the earlier actin-dependent processes that drive cup formation. The transition from PtdIns(3,4,5)P_3 to PtdIns3P on nascent macropinosomes constitutes the permissive signal for Phafin2 membrane engagement *via* its FYVE domain and oligomerization. This initial recruitment, however, could be subject to negative regulation through phosphorylation of the polyD motif [8,18] by an as-yet-unidentified serine/threonine kinase, which would restrain premature or excessive Phafin2 accumulation. While the upstream signaling cascades that initiate macropinocytosis, including Ras GTPase activation and PI3-kinase-dependent phosphoinositide production, have been extensively reviewed [31,32], the post-translational regulation of proteins operating at the macropinosome membrane during maturation remains poorly defined. An exception is the regulation of macropinosome contraction, which is mediated by the two-pore channel (TPC) through Na^+ efflux and Cl^- channel activity, driving osmotic water loss and reduction of intravesicular hydrostatic pressure [31]. TPC activity is itself subject to dual phosphoinositide- and kinase-dependent control. PtdIns(3,5)P_2, generated by the PIKfyve kinase, activates TPC and promotes macropinosome shrinkage, whereas mTOR-mediated phosphorylation of TPC under nutrient-replete conditions suppresses this

activity, thereby inhibiting macropinocytosis [31]. Phosphorylation-dependent control of membrane-binding effectors such as Phafin2 has not been addressed, representing a significant gap in our mechanistic understanding of macropinosome fate determination. The subsequent coincidence detection of PtdIns3P and PtdIns4P by the FYVE and PH domains, respectively, couples Phafin2 scaffolding activity to a defined maturation state. This dual-lipid requirement provides both specificity and cooperativity. Neither lipid alone is sufficient to sustain the high-density Phafin2 assemblies required for efficient oligomerization, whereas their co-occurrence stabilizes. In our reconstituted system, PtdIns3P alone supports only partial binding and tethering, whereas the two lipids together markedly enhance binding and liposome tethering. Because dual-lipid engagement coincides with non-fusogenic vesicle contact in cells [5], it may hold first-phase macropinosomes in a tethered, fusion-restricted state. Their co-occurrence may also stabilize extended oligomeric scaffolds that could impose curvature on the macropinosomal membrane and contribute to the release of the nascent macropinosome from the dense actin network.

Material and Methods

Chemicals. A synthetic polypeptide representing the human Phafin2 polyD motif (residues 240-DDDDDDDSSD-249) was purchased from Biomatik Corporation (Canada).

Protein expression and purification. The full-length human Phafin2 cDNA (residues 1-249) was cloned into the pGEX4T3 vector (Cytiva). The coding region for the PH domain of Phafin2 (residues 1-135) was subcloned into the pGEX6P1 vector, whereas the FYVE domain (residues 145–212) was cloned into pGEX4T3. The coding region for the human AKT1 PH domain (residues 1-111) was cloned into the pGEX4T1 vector. All constructs were transformed into *Escherichia coli* Rosetta cells (Stratagene) for recombinant protein expression. Cultures were grown in LB medium at 37°C until the optical density at 600 nm reached ~ 0.8. Recombinant protein expression was induced with 1 mM isopropyl β-D-1-thiogalactopyranoside, followed by incubation for 3 h at 25°C. Cell pellets were resuspended in extraction buffer (50 mM Tris-HCl, 500 mM NaCl, pH 7.3) supplemented with 10 mM benzamidine, 20 mM dithiothreitol (DTT), 0.25 mg/mL lysozyme, and 0.5% Triton X-100. Cells were lysed by sonication, and lysates were clarified by centrifugation at 17,420 × *g*. The resulting supernatant was incubated with glutathione-Sepharose 4B beads (Cytiva) for 1–2 h at 4°C with gentle rocking. After extensive washing, the GST fusion tags were cleaved overnight at 4°C using either thrombin (for pGEX4T1 and pGEX4T3 constructs) or HRV 3C protease (for pGEX6P1 constructs). The cleaved proteins were further purified by size-exclusion chromatography on a Superdex 75 column (Cytiva) pre-equilibrated with buffer containing 50 mM Tris-HCl and 1 M NaCl (pH 7.0). Fractions containing highly purified recombinant protein were pooled, concentrated, and stored at -80°C. Protein concentrations were determined by measuring absorbance at 280 nm using a NanoDrop One spectrophotometer (Thermo Fisher Scientific, Waltham, MA). Purity and integrity were evaluated by SDS-PAGE, in which 10 µg of each protein sample was analyzed alongside purified GST as a control.

ITC measurements. ITC experiments were carried out using a MicroCal PEAQ-ITC instrument (Malvern Panalytical Inc.) at 25°C. All samples were prepared in a buffer containing 20 mM HEPES (pH 7.3) and 100 mM NaCl. The polyD peptide was dissolved in the same buffer and adjusted to pH 7.0 to match the protein sample conditions. For each experiment, 50 μM of either wild-type or mutant Phafin2 PH domain was loaded into the ITC sample cell and titrated with 1–3 mM polyD peptide contained in the injection syringe. The titration protocol consisted of an initial delay of 10 min, followed by a preliminary 0.4 μL injection and 13 consecutive injections of 3 μL each, with 120-second intervals between injections and a constant stirring speed of 750 rpm. To correct for heat of dilution, control titrations of polyD peptide into buffer were subtracted from the experimental data. The resulting binding isotherms were analyzed using the MicroCal PEAQ-ITC analysis software, applying a one-site binding model. The reported K_D represents the mean value obtained from three independent experiments.

Tryptophan fluorescence. Intrinsic tryptophan fluorescence emission spectra of the Phafin2 PH domain were recorded at room temperature using a Jasco J-815 spectropolarimeter (Jasco, Easton, MD). Protein samples (0.25 μM) were prepared in a buffer containing 5 mM sodium citrate and 50 mM potassium fluoride at pH 7.3. Fluorescence emission spectra were collected using an excitation wavelength of 295 nm, with emission scanned from 310 to 410 nm in a 10-mm path length quartz cuvette. Titration experiments were conducted by stepwise addition of increasing concentrations of polyD peptide (2–30 μM) to the protein sample. The resulting emission spectra were analyzed to evaluate binding-induced spectral changes. Data analysis was performed using GraphPad Prism software, version 8 (GraphPad Software, San Diego, CA).

NMR spectroscopy. NMR experiments were performed at 25°C on a Bruker Avance III 600 MHz spectrometer (Bruker BioSpin, Billerica, MA) equipped with a 5 mm z-gradient triple resonance probe, located at the Virginia Tech NMR Facility. ^{1}H-^{15}N Phafin2 PH domain was prepared at a final concentration of 150 μM in a buffer containing 90% H_2O/10% D_2O, 20 mM d_{11}Tris-HCl (pH 7.0), 100 mM NaCl, 1 mM d_{18} DTT, and 1 mM NaN_3. The polyD peptide was dissolved in the same buffer and adjusted to pH 7.0. Two-dimensional ^{1}H–^{15}N heteronuclear single quantum coherence (HSQC) spectra were acquired for the ^{15}N-labeled Phafin2 PH domain both in the absence and presence of 1.2 mM polyD peptide. NMR data were processed as described [33] and analyzed using Mnova software (Mestrelab Research, Santiago de Compostela, Spain).

HDX-MS data collection and analysis. HDX-MS was performed at the Biomolecular and Proteomics Mass Spectrometry Facility (BPMSF) of the University California San Diego, using a Waters Synapt G2Si system with HDX technology (Waters Corporation) according to methods previously described [34]. Deuterium exchange reactions were performed using a Leap HDX PAL autosampler (Leap Technologies, Carrboro, NC). D_2O buffer was prepared by lyophilizing the indicated proteins in 20 mM HEPES, pH 7.3, 150 mM NaCl, initially dissolved in ultrapure water, and redissolving the powder in the same volume of 99.96% D_2O (Cambridge Isotope Laboratories, Inc., Andover, MA) immediately before use. Deuterium exchange was measured in triplicate at each time point (0, 0.5, 1, 2, and 5 min). For each deuteration

time point, 4 µL of protein was held at 25°C for 5 min before being mixed with 56 µL of D_2O buffer. The deuterium exchange was quenched for 2 min at 1°C by combining 50 µL of the deuteration reaction with 50 µL of 0.25M TCEP, final pH 2.66. The quenched sample (90 µL) was then injected in a 100 µL sample loop, followed by digestion on an in-line pepsin column (Immobilized Pepsin, Pierce) at 15°C. The resulting peptides were captured on a BEH C18 Vanguard precolumn, separated by analytical chromatography (Acquity UPLC BEH C18, 1.7 µm 1.0 × 50 mm, Waters Corporation) using a 7–85% acetonitrile gradient in 0.1% formic acid over 7.5 min, and electrosprayed into the Waters Synapt G2Si quadrupole time-of-flight mass spectrometer. The mass spectrometer was set to collect data in the Mobility, ESI+ mode; mass acquisition range of 200–2000 (m/z); scan time 0.4 s. Continuous lock mass correction was accomplished with infusion of leu-enkephalin (m/z = 556.277) every 30 s (mass accuracy < 1 ppm for calibration standard). For peptide identification, the mass spectrometer was set to collect data in mobility-enhanced data-independent acquisition (MS^E), mobility ESI+ mode instead. Peptide masses were identified from triplicate analyses and data were analyzed using the ProteinLynx global server (PLGS) version 3.0.3 (Waters Corporation). Peptide masses were identified using a minimum number of 250 ion counts for low energy peptides and 50 ion counts for their fragment ions; the peptides also had to be larger than 1,500 Da. The following cutoffs were used to filter peptide sequence matches: minimum products per amino acid of 0.2, minimum score of 7, maximum MH+ error of 5 ppm, and a retention time RSD of 5%. In addition, the peptides had to be present in two of the three ID runs collected. The peptides identified in PLGS were then analyzed using DynamX 3.0 data analysis software (Waters Corporation). The relative deuterium uptake for each peptide was calculated by comparing the centroids of the mass envelopes of the deuterated samples with the undeuterated controls following previously published methods [35]. The peptides reported on the coverage maps are those from which data were obtained. Data are represented as mean values ± SEM of three technical replicates due to processing software limitations, however the LEAP robot provides highly reproducible data for biological replicates. The deuterium uptake was corrected for back-exchange using a global back exchange correction factor (typically ~ 25%) determined from the average percent exchange measured in disordered termini of various proteins [36]. ANOVA analyses and t tests with a p value cutoff of 0.05 implemented in the program, DECA, were used to determine the significance of differences between HDX data points [37]. Deuterium uptake plots were generated in DECA (github.com/komiveslab/DECA) and the data are fitted with an exponential curve for ease of viewing.

Liposome co-sedimentation assay. Lipids were prepared with the following compositions: no phosphoinositides (control), 2% PtdIns3P, 5% PtdIns4P, or a combination of 2% PtdIns3P and 5% PtdIns4P. The remaining lipid content, including that of the control condition, consisted of 70% 1,2-dioleoyl-sn-glycero-3-phosphocholine and 30% 1,2-dioleoyl-sn-glycero-3-phosphoethanolamine (both from Avanti Polar Lipids). Lipid mixtures were vortexed and sonicated three times in 2-second intervals, ending with a final vortex. To form a thin lipid film, organic solvents were evaporated under a stream of liquid nitrogen while rotating the vial at a 45° angle. The lipid film was then dried overnight in a vacuum desiccator. Hydration of the lipid film was performed using prewarmed buffer (72°C) containing 20 mM HEPES (pH 7.3) and 100 mM NaCl, followed by incubation for 1 h at 72°C. Liposomes were subjected to

five freeze-thaw cycles, alternating between liquid nitrogen (20 s) and a 72°C water bath (3 min), and then extruded with polycarbonate membranes with pore sizes ranging from 50 to 400 nm (Avanti Polar Lipids). For protein binding assays, 20 µg of protein was incubated with liposomes (2 mg/ml) at room temperature for 1 h on a rotor. Liposome-bound protein was separated by ultracentrifugation at 180,000 x*g* for 1 h at 21°C (Beckman Coulter). Pellet and supernatant fractions were analyzed by SDS-PAGE. Uncropped gels are shown in **Suppl. Figure 9**.

Chemical crosslinking. Chemical crosslinking was performed using bis(sulfosuccinimidyl) suberate (BS^3; Thermo Scientific) dissolved to 9 mM in buffer containing 20 mM HEPES (pH 7.3) and 100 mM NaCl. Liposomes of different compositions were prepared as described for the liposome co-sedimentation assay. Protein (10 µg) was diluted in the same buffer and incubated with liposomes (100 µg) in a final volume of 80 µL for 30 min at room temperature. BS^3 was then added to a final concentration of 1 mM, and the reactions were incubated for an additional 30 min at room temperature. Reactions were quenched with 40 mM Tris-HCl, pH 8, for 15 min and analyzed by SDS-PAGE. Uncropped gels are shown in **Suppl. Figure 9**.

Computational analysis. The AlphaFold-predicted structure of human Phafin2 (Entry AF-Q9H8W4-F1) served as the starting model for all simulations. The PH domain, FYVE domain, and C-terminal tail were defined as residues 1-135, 145–212, and 213–249, respectively; the polyD region spans residues 240–249. Two systems were prepared for comparative analysis: nonphosphorylated Phafin2 and a phosphorylated variant in which S239, S247, and S248 were modified accordingly. Normal mode analysis (NMA) was carried out using the anisotropic network model (ANM) implemented in ProDy [38]. Tail-containing and tailless models were compared to evaluate the contribution of the C-terminal tail to PH-FYVE interdomain motion. For each model, conformational variation along Mode 1 was characterized by measuring the center-of-mass distance between the PH and FYVE domains and the inter-domain axial angle across the ensemble of generated conformers. Electrostatic potential calculations for nonphosphorylated and phosphorylated Phafin2 were performed using DelPhi [39]. This tool solves the Poisson-Boltzmann equation by finite difference method to calculate electrostatic potential ϕ(r):

$$\nabla \bullet \left[\epsilon\left(\mathrm{r}\right)\nabla\,\phi\ \left(\mathrm{r}\right)\right] = -4\pi\,\rho\ \left(\mathrm{r}\right) + \epsilon\left(\mathrm{r}\right)\kappa^{\,2}\left(\mathrm{r}\right)\sinh\left(\frac{\square\left(\mathrm{r}\right)}{k_B T}\right)$$

1

where ρ(r) is the permanent charge density, ε(r) is the dielectric permittivity, *T* is temperature, *κ* is the Debye-Huckel parameter, and k_B is the Boltzmann constant. Electrostatic potential maps were visualized in UCSF Chimera [40], with positively and negatively charged regions rendered in blue and red, respectively, over a color scale of − 3.0 to + 3.0 kT/e. To examine the electrostatic properties of the PH-FYVE interface, surface representations were generated both with and without the polyD tail included in the surface calculation. MD simulations of nonphosphorylated and S239/S247/S248-phosphorylated Phafin2 were carried out using NAMD [41] with explicit solvent at the Texas Advanced Computing Center

(TACC; http://www.tacc.utexas.edu). Each system was simulated for 20 ns in the presence of 150 mM NaCl. Structural stability was assessed by RMSD, and residue-level flexibility was evaluated by RMSF. Salt bridges and hydrogen bonds between the polyD tail and the PH–FYVE interface were analyzed over the equilibrated portion of each trajectory (10–20 ns). Salt-bridge occupancy was determined for oppositely charged residue pairs using a distance cutoff of 4.0 Å [42], and hydrogen bonds were identified using a distance cutoff of 4.0 Å and an angle cutoff of 20° [43]. For both interaction types, occupancy was calculated as the percentage of analyzed frames in which a given interaction was present.

Confocal imaging. Liposomes containing 5% 1,2-dioleoyl-sn-glycero-3-phosphoethanolamine-N-(carboxyfluorescein), either lacking or containing the indicated phosphoinositides, were prepared by extrusion using 800 nm polycarbonate membranes and incubated with 2 μM of the indicated proteins. Confocal microscopy was performed using a Nikon AXR point-scanning confocal system built around an inverted Ti2 Eclipse microscope. The system was equipped with a 488 nm excitation laser and an NSPARC array detector for imaging the vesicles. Liposomes were imaged using a 100×/1.45 oil objective lens with additional scan zoom to acquire z-stacks at a step size of 0.2–0.3 μm and/or timelapses with no delay or an interval of 5 s. Representative slices were processed using ImageJ v. 1.54p, cropped to the same area size. In some cases, a gamma adjustment of 1.1–1.3 was applied to enhance fluorescence localization differences within individual vesicles.

Declarations

Competing interests

The authors declare no competing financial interest.

Funding

for this study was provided by the Dean Discovery Funds of Virginia Tech (D.G.S.C.). Additional support was received from the National Science Foundation (Grant 2337495) awarded to D.G.S.C. The BPMSF-University California San Diego Facility is supported by the NIH shared instrumentation grant numbers S10 OD016234 (Synapt-HDX-MS) and S10 OD021724 (LUMOS Orbi-Trap). The Facility for Advanced Imaging and Microscopy is supported by RRID: SRC_027348.

Author Contribution

D.G.S.C. conceived the project. M.C. and T.T. designed constructs. M.C. performed and analyzed liposome co-sedimentation assays, circular dichroism, trypsin-limited proteolysis, and crosslinking assays. M.C., T.T., and M.H. performed ITC experiments. T.T. performed tryptophan fluorescence assays. T.T. and M.H., performed NMR experiments. L.L. designed molecular dynamics simulations. W.G.

performed molecular dynamics simulations and analyzed simulation trajectories. E.N. collected and analyzed the liposome confocal images. D.G.S.C. supervised the study. D.G.S.C. drafted the manuscript and all authors contributed to editing and approved the final version.

Acknowledgement

Funding for this study was provided by the Dean Discovery Funds of Virginia Tech (D.G.S.C.). Additional support was received from the National Science Foundation (Grant 2337495) awarded to D.G.S.C. The BPMSF-University California San Diego Facility is supported by the NIH shared instrumentation grant numbers S10 OD016234 (Synapt-HDX-MS) and S10 OD021724 (LUMOS Orbi-Trap). The Facility for Advanced Imaging and Microscopy is supported by RRID: SRC_027348.

Data availability

All data generated or analysed during this study are included in this published article (Supplementary Data 1 and 2).

References

1. Palmulli, R. & Machesky, L.M. Is macropinocytosis more than just a passive gulp? *Curr Opin Cell Biol* 94, 102513(2025).
2. Tu, H., Wang, H. & Cai, H. Macropinocytosis: Molecular mechanisms and regulation. *Curr Opin Cell Biol* 95, 102563(2025).
3. Tang, T., Hasan, M. & Capelluto, D.G.S. Phafins Are More Than Phosphoinositide-Binding Proteins. *Int J Mol Sci* 24(2023).
4. Tang, T.X., Finkielstein, C.V. & Capelluto, D.G.S. The C-terminal acidic motif of Phafin2 inhibits PH domain binding to phosphatidylinositol 3-phosphate. *Biochim Biophys Acta Biomembr* 1862, 183230(2020).
5. Schink, K.O. et al. The phosphoinositide coincidence detector Phafin2 promotes macropinocytosis by coordinating actin organisation at forming macropinosomes. *Nat Commun* 12, 6577(2021).
6. Tan, K.W. et al. JIP4 is recruited by the phosphoinositide-binding protein Phafin2 to promote recycling tubules on macropinosomes. *J Cell Sci* 134, jcs258495(2021).
7. Freeman, S.A. et al. Lipid-gated monovalent ion fluxes regulate endocytic traffic and support immune surveillance. *Science* 367, 301–305(2020).
8. Olsen, J.V. et al. Quantitative phosphoproteomics reveals widespread full phosphorylation site occupancy during mitosis. *Sci Signal* 3, p. ra3(2010).
9. Matsuda-Lennikov, M. et al. Lysosomal interaction of Akt with Phafin2: a critical step in the induction of autophagy. *PLoS ONE* 9, e79795(2014).

10. Ellena, J.F., Tang, T.X., Shanaiah, N. & Capelluto, D.G.S. Backbone (1)H, (15)N, and (13)C resonance assignments of the Phafin2 pleckstrin homology domain. *Biomol NMR Assign* 16, 27–30(2022).
11. Kutateladze, T.G. Phosphatidylinositol 3-phosphate recognition and membrane docking by the FYVE domain. *Biochim Biophys Acta* 1761, 868–77(2006).
12. Bahar, I., Cheng, M.H., Lee, J.Y., Kaya, C. & Zhang, S. Structure-Encoded Global Motions and Their Role in Mediating Protein-Substrate Interactions. *Biophys J* 109, 1101–9(2015).
13. Zhang, Y. et al. Structural insights into membrane remodeling by SNX1. *Proc Natl Acad Sci U S A* 118(2021).
14. Sakamoto, Y. et al. The Nedd4L ubiquitin ligase is activated by FCHO2-generated membrane curvature. *EMBO J* 43, 5883–5909(2024).
15. Okedigba, A.O. et al. Soybean Lectin Cross-Links Membranes by Binding Sulfatide in a Curvature-Dependent Manner. *J Agric Food Chem* 73, 14020–14031(2025).
16. Kerr, M.C. & Teasdale, R.D. Defining macropinocytosis. *Traffic*10, 364–71 (2009).
17. Tang, T.X. et al. Structural, thermodynamic, and phosphatidylinositol 3-phosphate binding properties of Phafin2. *Protein Sci* 26, 814–823(2017).
18. Sharma, K. et al. Ultradeep human phosphoproteome reveals a distinct regulatory nature of Tyr and Ser/Thr-based signaling. *Cell Rep* 8, 1583–94(2014).
19. Kutateladze, T.G. et al. Multivalent mechanism of membrane insertion by the FYVE domain. *J Biol Chem* 279, 3050–7(2004).
20. Powis, G., Meuillet, E.J., Indarte, M., Booher, G. & Kirkpatrick, L. Pleckstrin Homology [PH] domain, structure, mechanism, and contribution to human disease. *Biomed Pharmacother* 165, 115024(2023).
21. Balla, T. Phosphoinositides: tiny lipids with giant impact on cell regulation. *Physiol Rev* 93, 1019–137(2013).
22. Madani, M. & Tarakanova, A. Advancements in characterization of protein dynamics with machine learning. *Soft Matter* 2, 1–27(2026).
23. Hasan, M. & Capelluto, D.G.S. The PH Domain and C-Terminal polyD Motif of Phafin2 Exhibit a Unique Concurrence in Animals. *Membranes (Basel)* 12(2022).
24. Saei, A.A. et al. System-wide identification and prioritization of enzyme substrates by thermal analysis. *Nat Commun* 12, 1296(2021).
25. Alessi, D.R. et al. Mechanism of activation of protein kinase B by insulin and IGF-1. *EMBO J* 15, 6541–51(1996).
26. Zhao, X. et al. Membrane targeting of TIRAP is negatively regulated by phosphorylation in its phosphoinositide-binding motif. *Sci Rep* 7, 43043(2017).
27. Eitzen, G., Smithers, C.C., Murray, A.G. & Overduin, M. Structure and function of the Fgd family of divergent FYVE domain proteins (1). *Biochem Cell Biol* 97, 257–264(2019).

28. Lenoir, M. et al. Phosphorylation of conserved phosphoinositide binding pocket regulates sorting nexin membrane targeting. *Nat Commun* 9, 993(2018).
29. Yokogawa, M. et al. NMR analyses of the interaction between the FYVE domain of early endosome antigen 1 (EEA1) and phosphoinositide embedded in a lipid bilayer. *J Biol Chem* 287, 34936–45(2012).
30. Kutateladze, T.G. & Overduin, M. Structural mechanism of endosome docking by the FYVE domain. *Science* 291, 1793–6(2001).
31. Wu, Y., Hu, X., Wei, Z. & Lin, Q. Cellular Regulation of Macropinocytosis. *Int J Mol Sci* 25(2024).
32. Palm, W. Signaling Pathways that Regulate Macropinocytosis in Mammalian Cells. *Subcell Biochem* 98, 143–167(2022).
33. Xiao, S. et al. Structure, sulfatide binding properties, and inhibition of platelet aggregation by a disabled-2 protein-derived peptide. *J Biol Chem* 287, 37691–702(2012).
34. Peacock, R.B., Davis, J.R., Markwick, P.R.L. & Komives, E.A. Dynamic Consequences of Mutation of Tryptophan 215 in Thrombin. *Biochemistry* 57, 2694–2703(2018).
35. Wales, T.E., Fadgen, K.E., Gerhardt, G.C. & Engen, J.R. High-speed and high-resolution UPLC separation at zero degrees Celsius. *Anal Chem* 80, 6815–20(2008).
36. Ramsey, K.M., Dembinski, H.E., Chen, W., Ricci, C.G. & Komives, E.A. DNA and IkappaBalpha Both Induce Long-Range Conformational Changes in NFkappaB. *J Mol Biol* 429, 999–1008(2017).
37. Lumpkin, R.J. & Komives, E.A. DECA, A Comprehensive, Automatic Post-processing Program for HDX-MS Data. *Mol Cell Proteomics* 18, 2516–2523(2019).
38. Zhang, S. et al. ProDy 2.0: increased scale and scope after 10 years of protein dynamics modelling with Python. *Bioinformatics* 37, 3657–3659(2021).
39. Li, L. et al. DelPhi: a comprehensive suite for DelPhi software and associated resources. *BMC Biophys* 5, 9(2012).
40. Pettersen, E.F. et al. UCSF Chimera–a visualization system for exploratory research and analysis. *J Comput Chem* 25, 1605–12(2004).
41. Phillips, J.C. et al. Scalable molecular dynamics with NAMD. *J Comput Chem* 26, 1781–802(2005).
42. Sanchez, J. et al. Salt Bridge Builder: Using Residue Distances to Predict Salt Bridge Formation. *J Chem Inf Model* 66, 4975–4990(2026).
43. Guo, W. et al. Using a comprehensive approach to investigate the interaction between Kinesin-5/Eg5 and the microtubule. *Comput Struct Biotechnol J* 20, 4305–4314(2022).

Figures

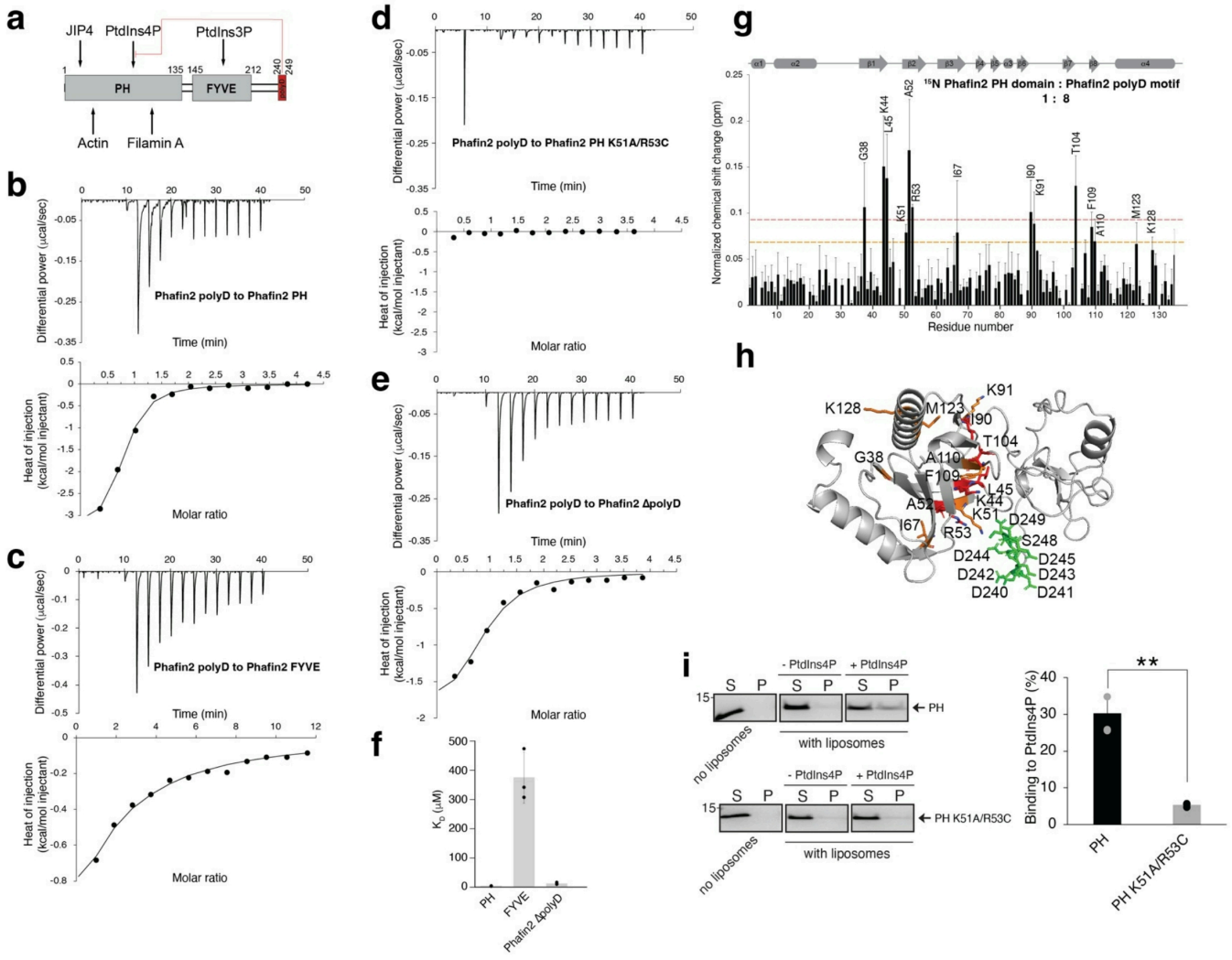

Figure 1

The Phafin2 PH domain directly binds the polyD motif. (**a**) Schematic of Phafin2 domain organization. Binding partners and their corresponding interaction regions are indicated. (**b-e**) ITC thermograms (upper panels) and binding isotherms (lower panels) for titration of Phafin2 polyD peptide into Phafin2 PH (**b**), Phafin2 FYVE (**c**), Phafin2 PH K51A/R53C (**d**), and Phafin2 ΔpolyD (**e**). Each panel depicts a representative thermogram from three independent titration experiments. (**f**) Plot representing the estimated dissociation constant (K_D) for the above Phafin2 constructs for the polyD motif. (**g**) Plot of normalized chemical shift perturbations (Δδ) of backbone amides in the Phafin2 PH domain upon titration with the polyD motif peptide. The orange and red dashed lines indicate thresholds of Δδ average + 1.0 × SD and Δδ average + 1.5 × SD, respectively. (**h**) Ribbon representation of the Phafin2 PH domain highlighting residues exhibiting significant chemical shift perturbations upon polyD motif binding, mapped in green. The structural model of Phafin2 was obtained from AlphaFold. (**i**) Left, binding of Phafin2 PH and PH K51A/R53C to 400-nm liposomes containing PtdIns4P. Right, densitometric quantification of the bound fraction. In all panels, S, supernatant; P, pellet. **, $p < 0.01$.

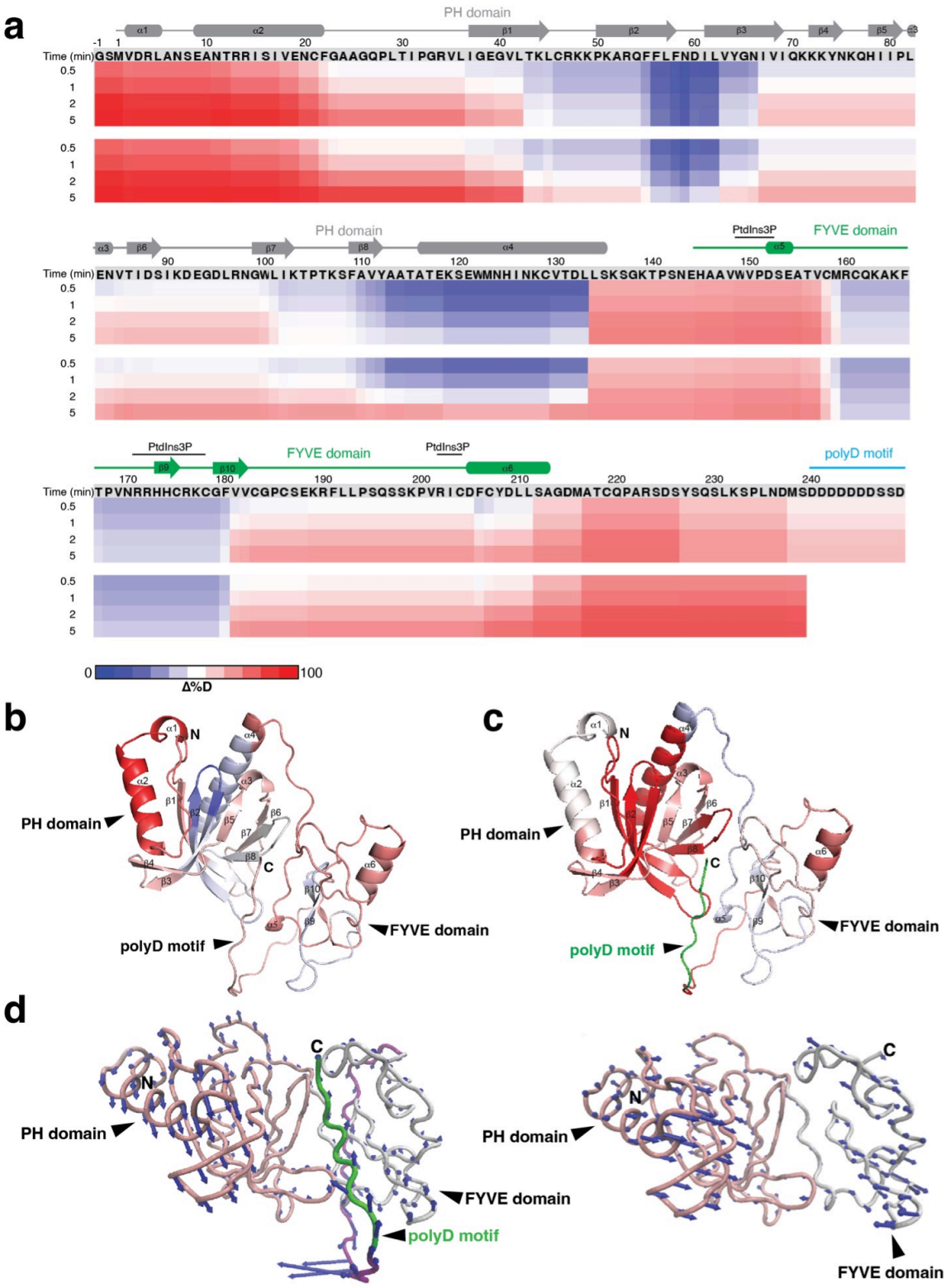

Figure 2

The PtdIns4P-binding site of the Phafin2 PH domain becomes solvent-exposed in the absence of the polyD motif. (**a**) Deuterium uptake heatmaps displayed along the Phafin2 primary sequence for Phafin2 (top set) and Phafin2 ΔpolyD (bottom set) at four exchange time points (0.5, 1, 2, and 5 min). Secondary structure as well as PtdIns3P-interacting regions are indicated above the sequence. The color scale represents the percentage of deuterium uptake (Δ%D) from 0 (blue) to 100 (red). (**b-c**) Ribbon

representations of the Phafin2 structure colored according to Δ%D values from HDX-MS data at the 5 min time point, for Phafin2 (**b**) and for the difference in deuterium incorporation between Phafin2 ΔpolyD and Phafin2 (**c**). (**d**) Representative normal mode displacement vectors for PH-FYVE models containing (left) or lacking (right) the C-terminal tail. Arrows indicate the direction and relative magnitude of collective motions. The PH domain, FYVE domain, C-terminal tail, and polyD motif are colored pink, gray, purple, and green, respectively.

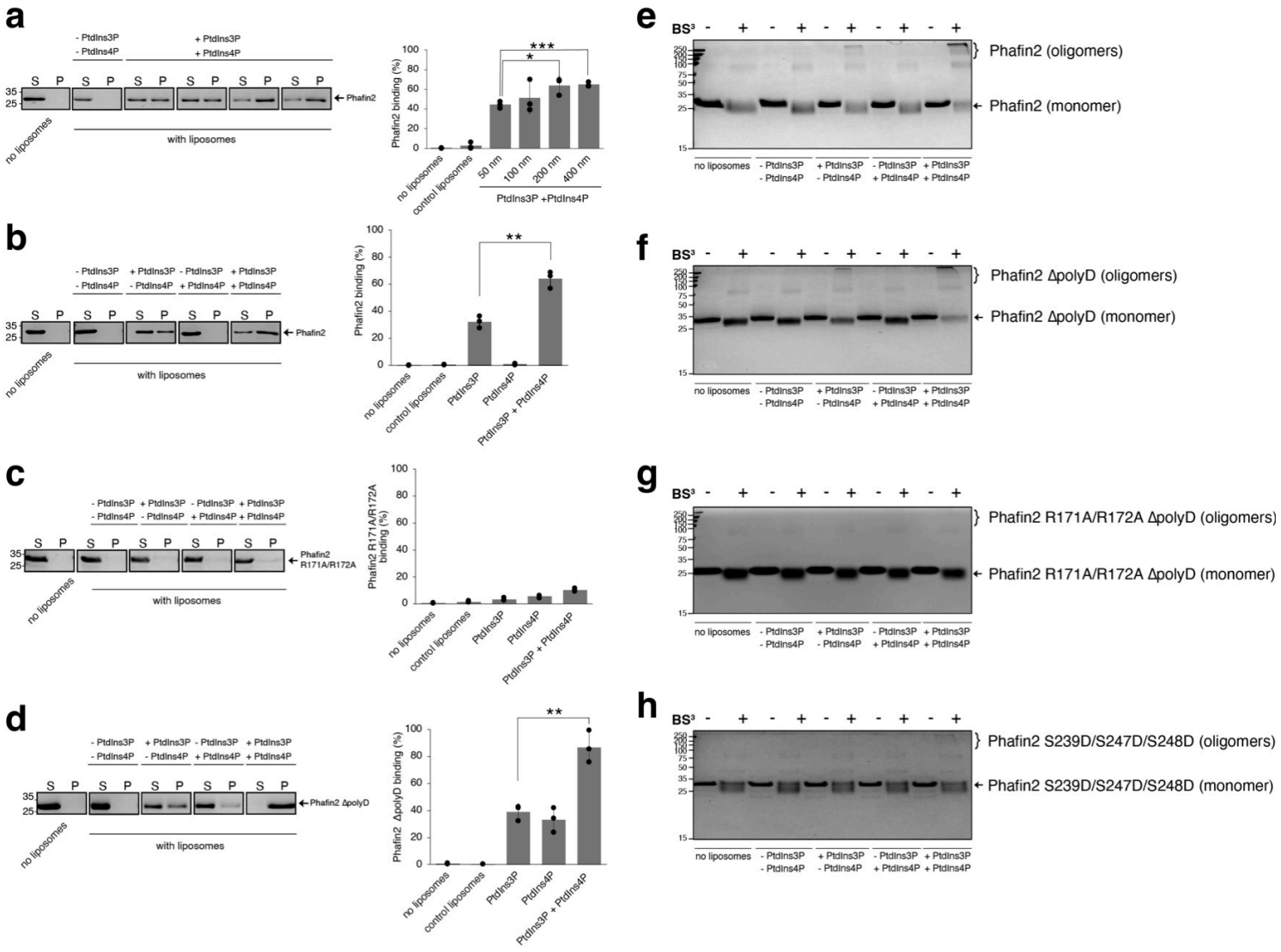

Figure 3

Intramolecular allosteric regulation and PtdIns3P-dependent oligomerization of Phafin2 mediated by the FYVE domain. (**a)** Left, binding of Phafin2 to the indicated liposome sizes containing both PtdIns3P and PtdIns4P. Right, densitometric quantification of the bound fraction. S, supernatant; P, pellet. *, $p < 0.1$; ***, $p < 0.001$. **(b-d**) Left, binding of Phafin2 (**b**), Phafin2 R171A/R172A (**c**) and Phafin2 ΔpolyD (**d)** to 400-nm liposomes containing the indicated phosphoinositides. Right, densitometric quantification of the bound fraction. In all panels, S, supernatant; P, pellet. **, $p < 0.01$. (**e-h**) Crosslinking assays of Phafin2 (**e**), Phafin2 ΔpolyD (**f**), Phafin2 R171A/R172A ΔpolyD (**g**), and Phafin2 S239D/S247D/S248D (**h**).

Constructs were incubated with the indicated liposomes in the absence or presence of BS³, and the samples were then run on SDS-PAGE

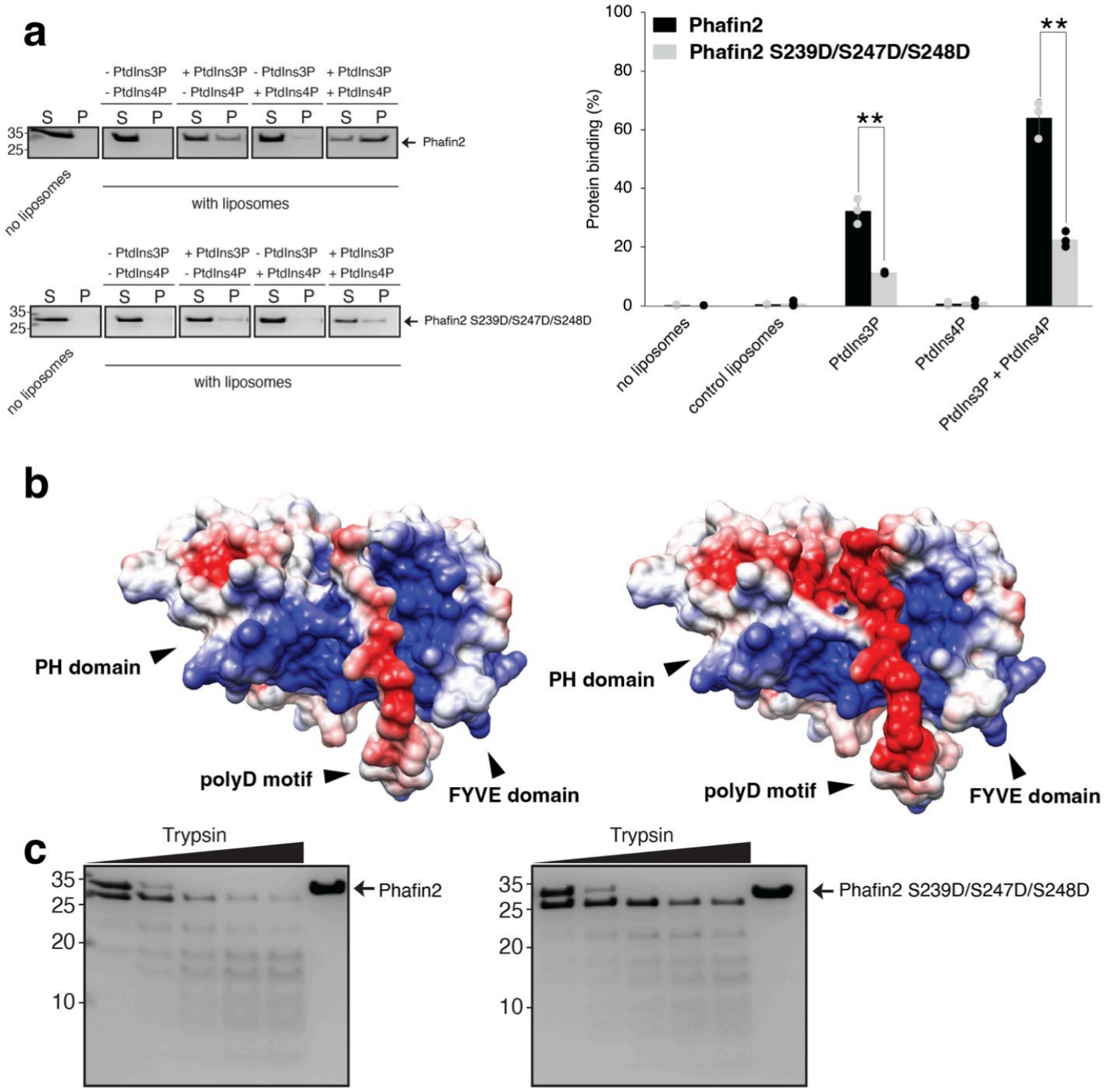

Figure 4

Phosphorylation of Phafin2 at the C-terminal tail modulates FYVE domain function. (**a**) Left, liposome co-sedimentation assays of Phafin2 (top) and Phafin2 S239D/S247D/S248D (bottom) using the indicated phosphoinositide compositions. Right, densitometric quantification of the bound fraction. In all panels, S, supernatant; P, pellet. **, $p < 0.01$. (**b**) Electrostatic surface potential of the non-phosphorylated

and phosphorylated Phafin2 models. The electrostatic potential is colored from −3 kT/e to +3 kT/e, with red and blue indicating negative and positive potential, respectively. (**c**) Trypsin-limited proteolysis of Phafin2 (left) and Phafin2 S239D/S247D/S248D (right) resolved by SDS-PAGE.

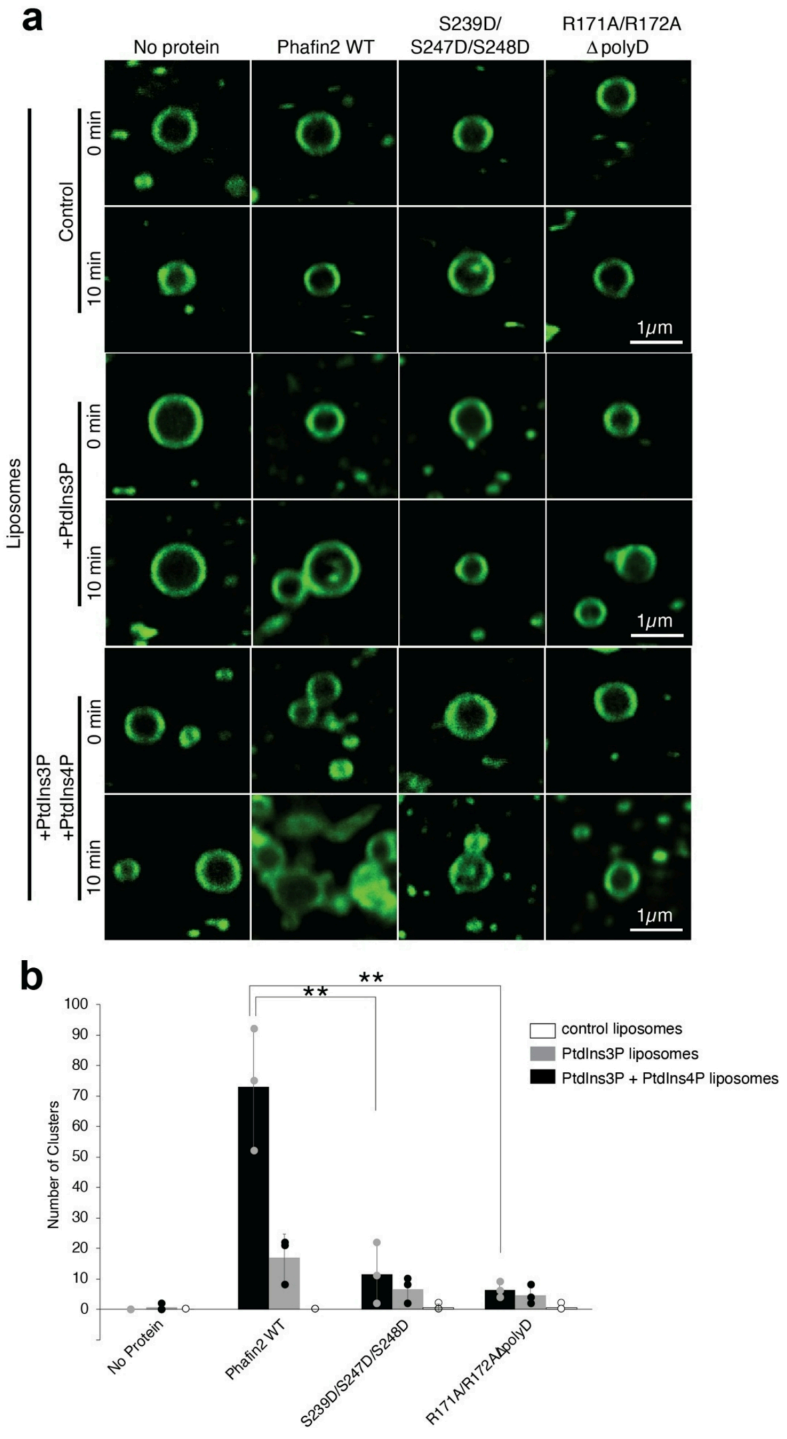

Figure 5

Phafin2 directly promotes PtdIns3P- and PtdIns4P-dependent vesicle tethering. (**a**) Confocal images of fluorescently labeled liposomes lacking or containing the indicated phosphoinositides after incubation with the indicated proteins for the indicated times. (**b**) Quantification of the number of clusters formed by 800 nm liposomes in the absence or presence of the indicated Phafin2 constructs. Liposomes contained no phosphoinositides, PtdIns3P, or PtdIns3P plus PtdIns4P. Data are mean ± s.d. from n = 3 independent experiments; **, p < 0.01.

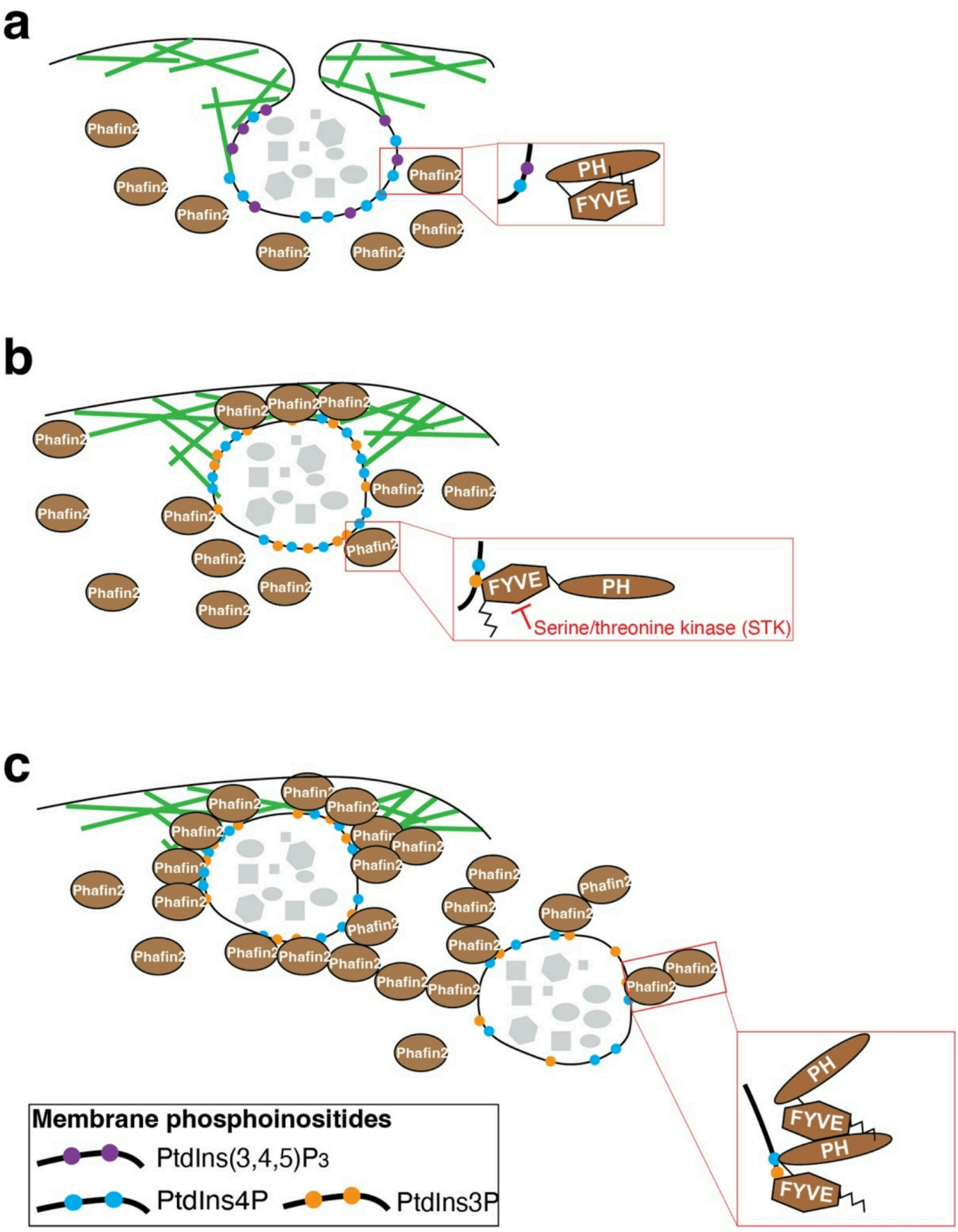

Figure 6

Schematic model of Phafin2 recruitment and membrane engagement during endosomal maturation. (**a**) During macropinocytic cup formation, PtdIns(3,4,5)P_3 synthesis and reorganization of actin filaments underlying the plasma membrane drive uptake of fluid and macromolecules. Closure of the macropinocytic cup is accompanied by actin polymerization and PtdIns4P accumulation at the plasma membrane. Autoinhibition of the PH domain by the polyD motif prevents Phafin2 PtdIns4P-dependent membrane targeting. (**b**) PtdIns3P production on nascent macropinosomes enables Phafin2 to adopt an open conformation and associate with the membrane *via* its FYVE domain, stimulating Phafin2 oligomerization. The open conformation weakens the interaction between the PH domain and the polyD motif. Phosphorylation of the polyD motif by an unidentified serine/threonine kinase is proposed to downregulate this process by stabilizing FYVE-polyD interactions. (**c**) PtdIns4P present on macropinosomes engages the released PH domain, further enhancing Phafin2 oligomerization and membrane tethering.

Supplementary Files

This is a list of supplementary files associated with this preprint. Click to download.

- SupplementaryInformationCapelluto.docx